


Multiple first-order transitions in simplicial complexes on multilayer systemsSarika Jalan^{✉*} and Ayushi Suman[†]*Complex Systems Lab, Department of Physics, Indian Institute of Technology Indore,
Khandwa Road, Simrol, Indore-453552, India* (Received 13 June 2022; revised 9 August 2022; accepted 20 September 2022; published 21 October 2022)

The presence of higher-order interactions (simplicial complexes) on globally coupled systems yield abrupt first-order transitions to synchronization. We discover that simplicial complexes on multilayer systems can yield multiple basins of attraction, leading to multiple abrupt first-order transitions to (de)synchronization for associated coupled dynamics. Using the Ott-Antonsen approach, we develop an analytical framework for simplicial complexes on multilayer systems, reducing the high-dimensional evolution equation to a low-dimensional manifold, which thoroughly explains the origin and stability of all possible dynamical states, including multiple synchronization transitions. The study illustrating rich dynamical behaviors could be pivotal in comprehending the impacts of higher-order interactions on dynamics of complex real-world networks, such as brain, social, and technological, which have inherent multilayer architectures.

DOI: [10.1103/PhysRevE.106.044304](https://doi.org/10.1103/PhysRevE.106.044304)**I. INTRODUCTION**

Functional performances of a wide range of real-world complex systems, such as brain, social, and technological systems, are driven by underlying simplicial complexes defining higher-order interactions [1–5]. A simplicial complex of order one denotes pairwise interactions between a pair of nodes. Similarly, a simplicial of order 2 represents a set of three connected nodes forming a two-simplicial complex, and so on. Considering such higher-order interactions, aka simplicial complexes in interacting nonlinear dynamical units, has brought forward many emerging phenomena [6], among which, simplicial complexes that have been elucidated to lead the abrupt first-order transition to synchronization are of particular interest. Precisely, the simplicial complexes of order 2 or higher have been demonstrated to cause the first-order abrupt transition to synchronization in those systems which otherwise (i.e., only with pair-wise interactions) depict a smooth second-order transition to synchronization [7–10].

Furthermore, a set of nodes of a complex system connected through different types of interactions form a multilayer system. Investigations of real-world data, as well as both the numerical simulations and theoretical analysis of nonlinear models, have demonstrated that in complex systems represented by multilayer networks, activities of nodes in one layer, connected through one type of interaction, affect or govern dynamical activities of the nodes connected through other types of interactions in the other layers [11–14]. Similar to the first-order synchronization transition behavior exhibited by coupled dynamics on simplicial complexes, appropriate multilayering schemes have also been shown to lead to the abrupt first-order transition to synchronization in those networks which, in isolation, depict smooth second-order transition to synchronization [13,15,16].

This article discovers the existence of multiple basins of attractions yielding different routes to abrupt first-order transitions to synchronization in simplicial complexes on multilayer systems with each layer represented by a globally coupled network. Moreover, we develop a complete analytical framework using the Ott-Antonsen approach to analytically deduce the high-dimensional multilayer coupled dynamics to low-dimensional coupled equations for the associated order parameters of the individual simplicial layers. Such reduced time-dependent coupled equations for the simplicial layer's order parameters facilitate analytical demonstration of different routes to first-order transitions and calculations of different critical coupling strengths at which these transitions occur. Notably, using the Ott-Antonsen approach, we first derive the time-evolution equations for the order parameters of the simplicial complexes of coupled Kuramoto oscillators having pairwise (s_1), triadic (s_2), and tetra (s_3) interactions forming layers of the multilayer system. After that, we perform stability analysis for this set of the coupled differential equations at all their fixed points. The analytical calculations reveal the existence of one usual subcritical bifurcation leading to the first-order transition to synchronization, which is accompanied by hysteresis, and an abrupt transition to synchronization as a consequence of saddle-node bifurcation. Notably, depending upon the choice of the initial conditions, the setup leads to three additional saddle-node bifurcations, giving birth to another second-order transition to synchronization accompanied by a different critical coupling strength. We perform numerical experiments which comply with the analytical predictions.

II. MODEL AND RESULTS

Let us consider a multilayer system consisting of two layers. The N number of nodes in each layer interacts not only with the pairwise interactions (simplicial of order 1) but also through triangular (two-simplicial) and tetrahedral

*sarika@iiti.ac.in

†ayushishuman@gmail.com

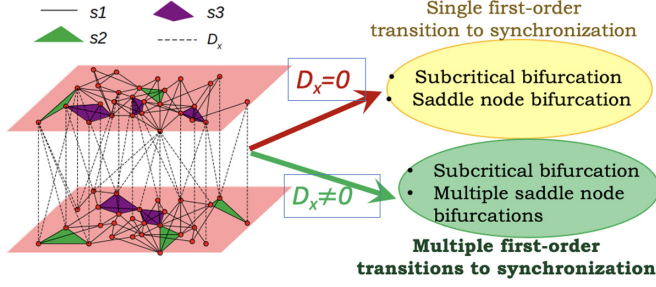


FIG. 1. Schematic diagram for (left) multilayer system consisting of simplicial layers, and (right) emerging dynamical phenomena in absence ($D_x = 0$) and in presence of multilayering ($D_x > 0$). Intra-layer connections are simplicial of orders 1, 2, and 3. Each node in the first layer is connected with all the nodes in the second layer with a multilayering strength D_x .

(three-simplicial) interactions (Fig. 1). The interlayer pairwise interactions are considered all-to-all, i.e., each node of the first simplicial layer interacts with all the nodes of the second simplicial layer with a strength D_x , referred to as multilayering strength. The dynamics of such a system can be studied with an extension of the Kuramoto-Sakaguchi model [17] given as

$$\dot{\theta}_i^{(k)} = \omega_i^{(k)} + \frac{D_x}{N} \sum_{j=1}^N \sin(\theta_j^{(k')} - \theta_i^{(k)}) + \hat{H}_i^{(k)}, \quad (1)$$

where

$$\begin{aligned} \hat{H}_i^{(k)} = & \frac{K_1^{(k)}}{N} \sum_{j=1}^N \sin(\theta_j^{(k)} - \theta_i^{(k)}) \\ & + \frac{K_2^{(k)}}{N^2} \sum_{j=1}^N \sum_{l=1}^N \sin(2\theta_j^{(k)} - \theta_l^{(k)} - \theta_i^{(k)}) \\ & + \frac{K_3^{(k)}}{N^3} \sum_{j=1}^N \sum_{l=1}^N \sum_{m=1}^N \sin(\theta_j^{(k)} + \theta_l^{(k)} - \theta_m^{(k)} - \theta_i^{(k)}). \end{aligned}$$

Here, the superscript $k(k')$, taking values 1 and 2, denotes the index of the layer under consideration, and $K_i^{(k)}$ indicates the overall coupling strength for the i -simplex interaction of the k th layer. In the respective mean fields, the dynamical evolution equations for the simplicial layers can be written as

$$\begin{aligned} \dot{\theta}_i^{(k)} = & \omega_i^{(k)} + K_1^{(k)} r_1^{(k)} \sin(\Psi_1^{(k)} - \theta_i^{(k)}) \\ & + K_2^{(k)} r_1^{(k)} r_2^{(k)} \sin(\Psi_2^{(k)} - \Psi_1^{(k)} - \theta_i^{(k)}) \\ & + K_3^{(k)} r_1^{3(k)} \sin(\Psi_1^{(k)} - \theta_i^{(k)}) \\ & + D_x r_1^{(k')} \sin(\Psi_1^{(k')} - \theta_i^{(k)}), \end{aligned} \quad (2)$$

with the complex order parameters of the k th simplicial layer defined as

$$z_n^{(k)} = r_n^{(k)} e^{i\Psi_n^{(k)}} = \frac{1}{N} \sum_{j=1}^N e^{in\theta_j^{(k)}}, \quad (3)$$

which measures the strength of global synchronization of the individual simplicial layers with $0 \leq r_n^{(k)} \leq 1$. $r_1^{(k)} \sim 0$

indicates a complete incoherent state, whereas $r_1^{(k)} \sim 1$ indicates global synchronization and $\Psi_1^{(k)}$ measures the mean phase of all the oscillators of the k th layer. In the absence of any higher-order interaction, Eq. (1) leads to a smooth second-order transition to synchronization for the individual layer [13], i.e., starting from an incoherent state corresponding to $r_1^{(k)} \sim 0$, after a critical coupling strength $r_1^{(k)}$ gradually increases to 1 with an increase in $K_1^{(k)}$. An introduction of the higher-order couplings (second and third terms in $\hat{H}_i^{(k)}$) brings about frustration in the system due to an interplay among the phases of three and four oscillators, respectively, for the triadic and tetrahedral term in the sinusoidal couplings. An increase in the pairwise intralayer coupling strength supports the overall coherence between the connected pairs of nodes. As soon as $K_1^{(k)}$ becomes strong enough to overcome the frustration caused by the higher-order interactions, there arises an abrupt first-order transition to the global synchronization. The implications of an inclusion of higher-order interactions in coupled Kuramoto oscillators interacting through simplicial complexes on single-layer networks are well-established, accompanied by rigorous analytical explanations [9]. Here, we consider systems in which simplicial layers are connected via interlayer connections and develop a full analytical framework to analyze the dynamical behavior of coupled Kuramoto oscillators on simplicial complexes on multilayer networks. We discover various emerging behaviors, namely, multiple first-order transitions to synchronization accompanied by different routes and basins of attraction, the existence of multiple saddle-node bifurcations in addition to the usual subcritical pitch-fork bifurcation, and a gradual shift from the first- to second-order transition to synchronization.

In the following, first we develop a rigorous analytical framework for the complete accomplishment of the coupled dynamical behaviors and their stability analyses. Then, we present numerical results obtained through the direct simulations of Eq. (1) to demonstrate a full match with the analytical calculations. We perform a linear stability analysis of the reduced equations (8) and explore the entire $r_1^{(1)} - r_1^{(2)}$ space. Further, we discuss the origin of the third bifurcation, followed by an analysis of the impacts of intralayer coupling strength of the second simplicial layer and interlayer coupling strengths on the nature of transitions in the first layer. Next, we present results for the dynamical evolution of the second layer and discuss how the origin of multiple transitions lies in the dynamical behaviors of the layer having only higher-order interactions.

A. Analytical derivation for dimension reduction to Ott-Antonsen manifold

Using the complex order parameters (3), Eq. (2) can be written as

$$\dot{\theta}_i^{(k)} = \omega_i^{(k)} + \frac{1}{N} (H^{(k)} e^{-i\theta_i^{(k)}} - H^{*(k)} e^{i\theta_i^{(k)}}), \quad (4)$$

with $H^{(k)} = K_1^{(k)} z_1^{(k)} + K_2^{(k)} z_2^{(k)} z_1^{*(k)} + K_3^{(k)} z_1^{2(k)} z_1^{*(k)} + D_x z_1^{(k')}$. In the thermodynamic limit $N \rightarrow \infty$, the state of the individual layer can be described by a density function $f^{(k)}(\theta^{(k)}, \omega^{(k)}, t)$ which measures the density of oscillators

with the phase between $\theta^{(k)}$ and $\theta^{(k)} + d\theta^{(k)}$ having a natural frequency lying between $\omega^{(k)}$ and $\omega^{(k)} + d\omega^{(k)}$ at time t for the k th layer. Since the number of oscillators in each layer is conserved, the density functions will individually satisfy the continuity equation:

$$0 = \frac{\partial f^{(k)}}{\partial t} + \frac{\partial}{\partial \theta^{(k)}} \left[f^{(k)} \left[\omega_i^{(k)} + \frac{1}{N} (H^{(k)} e^{-i\theta^{(k)}} - H^{*(k)} e^{i\theta^{(k)}}) \right] \right]. \quad (5)$$

Assuming the natural frequency $\omega^{(k)}$ of each oscillator drawn from a distribution $g(\omega^{(k)})$, the density function $f^{(k)}$ can be expanded into Fourier series as

$$\begin{aligned} f^{(k)}(\theta^{(k)}, \omega^{(k)}, t) \\ = \frac{g(\omega^{(k)})}{2\pi} \left[1 + \sum_{n=1}^{\infty} \hat{f}_n^{(k)}(\omega^{(k)}, t) e^{in\theta^{(k)}} + \text{c.c.} \right], \end{aligned}$$

where $\hat{f}_n^{(k)}(\omega^{(k)}, t)$ is the n th Fourier component and c.c. are the complex conjugates of the former terms. Next, we use the Ott-Antonsen [18] ansatz which assumes that all the Fourier modes decay geometrically, i.e., $\hat{f}_n^{(k)}(\omega^{(k)}, t) = \alpha^{n(k)}(\omega^{(k)}, t)$ for some function $\alpha^{(k)}$ which is analytic in the complex $\omega^{(k)}$ plane. After inserting the Fourier expansion of $f^{(k)}(\theta^{(k)}, \omega^{(k)}, t)$ in the continuity equation (5), the dynamics of the two-layer network collapses into a complex two-dimensional manifold (Ott-Antonsen manifold),

$$\dot{\alpha}^{(k)} = -i\omega^{(k)}\alpha^{(k)} + \frac{1}{2}[H^{(k)*} - H^{(k)}\alpha^{2(k)}], \quad (6)$$

with $H^{(k)}$ defined in Eq. (4). The order parameter in the thermodynamic limit can then be given as $z^{(k)} = \iint f^{(k)}(\theta^{(k)}, \omega^{(k)}, t) e^{i\theta^{(k)}} d\theta^{(k)} d\omega^{(k)}$, which after inserting the Fourier decomposition of $f^{(k)}$ becomes

$$z^{(k)} = \int \alpha^{(k)}(\omega^{(k)}, t) g(\omega^{(k)}) d\omega^{(k)}.$$

If we choose $g(\omega^{(k)})$ to be a Lorentzian frequency distribution $g(\omega^{(k)}) = \frac{\Delta^{(k)}}{\pi[\Delta^{2(k)} + (\omega^{(k)} - \omega_0^{(k)})^2]}$, where $\omega_0^{(k)}$ is mean and $2\Delta^{(k)}$ is full width at half maximum of the k th layer, $z^{*(k)}$ can be calculated by contour integration in the negative half complex plane, yielding, $z^{*(k)} = \alpha^{(k)}(\omega_0^{(k)} - i\Delta^{(k)}, t)$. For simplicity, we redefine the order parameters as $z^{(1)} = r e^{i\Phi}$ and $z^{(2)} = \rho e^{i\chi}$, Φ and χ being the mean phases of layers 1 and 2, respectively.

Upon scaling $\chi - \Phi$ as ξ , dimensionality of the system represented by Eq. (6) reduces to three:

$$\begin{aligned} \dot{r} &= -\Delta r + \frac{K_1^{(1)}}{2}[r - r^3] + \frac{K_{2+3}^{(1)}}{2}[r^3 - r^5] \\ &\quad + \frac{D_x}{2}[\rho - \rho r^2] \cos(\xi), \\ \dot{\rho} &= -\Delta \rho + \frac{K_1^{(2)}}{2}[\rho - \rho^3] + \frac{K_{2+3}^{(2)}}{2}[\rho^3 - \rho^5] \\ &\quad + \frac{D_x}{2}[r - r\rho^2] \cos(\xi), \\ \dot{\xi} &= \omega_0^{(2)} - \omega_0^{(1)} - \frac{D}{2} \left[2r\rho + \frac{r}{\rho} + \frac{\rho}{r} \right] \sin(\xi). \end{aligned} \quad (7)$$

In the steady state, $\dot{r} = \dot{\rho} = \dot{\xi} = 0$. Note that since this analytical derivation has considered the Cauchy frequency distribution centered at zero, for $\dot{\xi}$ to be zero, $\sin(\xi)$ has to be zero (since the quantity in square bracket cannot be zero). Which means $\chi = \Phi$, indicating synchronization of the mean phases of both the layers. Consequently, the above three coupled equations further reduce to

$$\begin{aligned} 0 &= -\Delta r + \frac{K_1^{(1)}}{2}[r - r^3] + \frac{K_{2+3}^{(1)}}{2}[r^3 - r^5] + \frac{D_x}{2}[\rho - \rho r^2], \\ 0 &= -\Delta \rho + \frac{K_1^{(2)}}{2}[\rho - \rho^3] + \frac{K_{2+3}^{(2)}}{2}[\rho^3 - \rho^5] + \frac{D_x}{2}[r - r\rho^2]. \end{aligned} \quad (8)$$

Equation (8) provides a solution to the dynamically stable states for the multilayer networks model (1) in terms of the order parameters of the individual simplicial layers (r and ρ). Ergo, a high-dimensional coupled dynamics is reduced to a two-dimensional evolution equation. This set of the coupled equations provides full understanding to the entire dynamics of the multilayer network model represented by Eq. (1).

B. Multiple first-order transitions and basins of attraction

The coupled dynamics [Eq. (1)] is evolved using the Runge-Kutta method of order 4, and after discarding an initial transient, the system settles to a stable state. Additionally, Eq. (8) is solved numerically, and steady-state behaviors of r and ρ are analyzed as a function of $K_1^{(1)}$. To comprehend the impact of dynamical behaviors of the nodes in one simplicial layer on those of the other layer, we freeze the coupling strengths of one layer (say, the second layer) to a set of values. Additionally, the simplicial coupling of the layers are fixed for all the results, unless stated otherwise. The frequency distribution in both layers for all numerical simulations are taken to be uniform Lorentzian distribution with mean 0 and $\Delta^{(k)} = 1$.

For the multilayer simplicial system, we discover multiple stable states accompanied by different basins of attraction which in turn yield different routes to the first-order transition to synchronization. Figure 2(a) depicts a very good match between the predictions based on the Ott-Antonsen method (8) and numerical evolution of the system Eq. (1). Note that the Ott-Antonsen manifold [Eq. (8)] has been derived analytically from Eq. (1). Further, these two coupled equations (low-dimensional manifold of $2N$ dimensional equations) are solved to obtain different curves referred as analytical predictions in figures.

Note that using the Ott-Antonsen approach analytically, we have performed dynamical reduction from $2N$ dimensional equations to two-dimensional Ott-Antonsen manifold [Eq. (8)]. First, we discuss the numerical results for the two-layer networks having all-to-all intralayer couplings. As illustrated in Fig. 2, depending upon the initial conditions, there exist different routes to the first-order transitions and various bifurcations. (1) The phase of the oscillators in both layers are randomly distributed in $[0 : \pi]$. For this set of initial conditions [green open square Fig. 2(a)] and $K_1^{(1)}, K_2^{(1)}, K_3^{(1)}$, taking any positive small values leads to $r = 0$ as a stable solution. Upon increasing $K_1^{(1)}$, there occurs a usual first-order

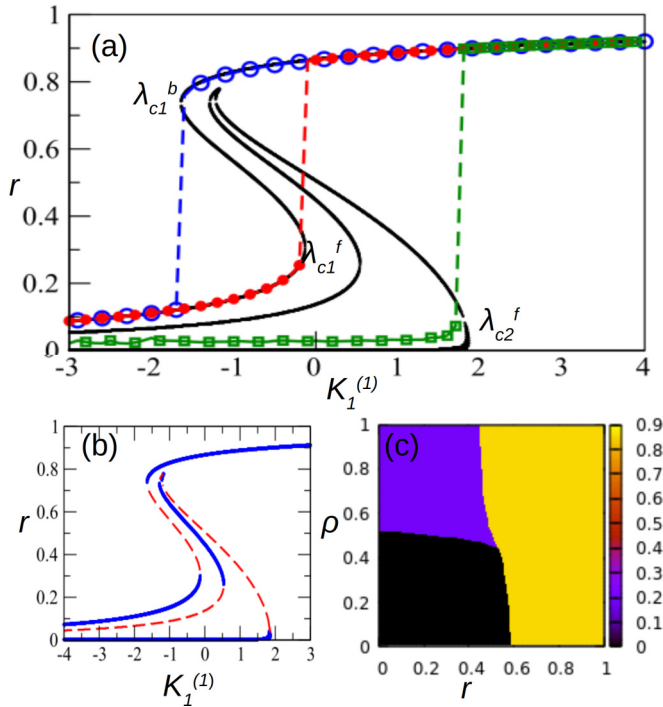


FIG. 2. Multiple synchronization transitions or multistability along with analytical predictions [Eq. (8)]. (a) Open circles (blue) indicate adiabatic backward while closed circles (red) represent adiabatic forward direction, both combined making HT (see text). Open squares (green) indicate forward direction corresponding to the random initial conditions, also referred as WHT (see text). Solid lines are numerical solutions of Eq. (8). (b) Stability diagram: Solid (blue) and dashed (red) lines, respectively, indicate stable and unstable manifolds. The stable blue curve in the middle is stable only in r and ρ direction and unstable in third ξ direction. (c) Basins of attraction for the entire $r - \rho$ space, depicting three stable regions for Eq. (7) for all possible initial conditions for r and ρ . At $K_1^{(1)} = -1$, black, grey (purple), and white (yellow) correspond to the green open square, red closed circle, and blue open circle, respectively, in (a). $N = 1000$, and $K_{2+3}^{(1)} = K_{2+3}^{(2)} = K_{2+3} = 10$ for all the simulations results. Here $D_x = 0.5$.

transition to synchronization at a critical coupling strength ($K_1^{(1)} = \lambda_{c2}^f$) as a consequence of the subcritical bifurcation as also observed for the isolated simplicial layer case [9]. (2) The initial condition corresponding to the synchronized state ($\theta_i = \theta_j, \forall i, j$) which is achieved for sufficiently large $K_1^{(1)}$ values. Starting from this initial condition, as $K_1^{(1)}$ decreases adiabatically, the dynamical evolution of the first simplicial layer lies in the coherent region (blue open circles) until the critical coupling strength ($K_1^{(1)} = \lambda_{c1}^b$), where the stable coherent state loses its stability as a consequence of a saddle-node bifurcation. The trajectory jumps to a far distant attractor corresponding to a state having r value close to zero and referred as weakly synchronized (or weakly coherent) state (blue open circles). This weakly synchronized state persists as $K_1^{(1)}$ decreases further. (3) The initial condition corresponding to this weakly synchronized state (blue open circles), which was achieved in the backward direction. Upon increasing $K_1^{(1)}$ adiabatically from this initial condition, the order parameter trajectory takes a different route than was followed while $K_1^{(1)}$

was decreasing. The coupled dynamics keeps depicting the weakly coherent behavior beyond λ_{c1}^b until a specific value of $K_1^{(1)}$ (red closed circles). At λ_{c1}^f , this weakly coherent stable state loses its stability again as a consequence of a saddle-node bifurcation and giving birth to the first-order transition to the coherent state.

Since this study demonstrates the existence of multiple synchronization transitions as the prime result, we refer to the transition corresponding to the hysteresis as HT and the transition without hysteresis as WHT. Therefore, in Fig. 2(a), blue open circles and solid lines correspond to backward HT, red closed circles and dashed lines correspond to forward HT, whereas green open squares correspond to WHT.

C. Origin of the third bifurcation

Equation (8) is numerically solved to obtain all the bifurcating lines depicted in Fig. 2(b). Furthermore, we perform the linear stability analysis around all the fixed points of Eq. (6) by evaluating the respective Jacobian matrices. A fixed point is asymptotically stable if both the eigenvalues of the corresponding Jacobian matrix have negative real parts [solid blue line in Fig. 2(b)], and it is unstable if at least one eigenvalue has a positive real part [red dashed line in Fig. 2(b)]. In addition to the stable manifold observed numerically (blue solid line), there exist three unstable manifolds (red dashed line) and one more stable manifold (blue solid line in the middle of two dashed red lines) which were not observed numerically. Upon analyzing a cross section at $\xi = 0$ corresponding to $K_1^{(1)} = -0.5$, one finds the existence of four stable manifolds. However, one stable state here corresponds to the out-of-phase-synchronized solution between the layers and is unstable in the ξ direction, and hence numerically infeasible. Therefore, this curve is not realized numerically from the reduced coupled mean-field equations, which is solved for $\xi = 0$. Figure 2(c) plots the basins of attraction for different regions, in which only three stable regions are visible for $K_1^{(1)} = -1$. (c) is plotted in the r - ρ parameter regime. To obtain the initial conditions for phases corresponding to a specific set of values of r or ρ , one can use an asymmetry parameter η such that $N\eta$ oscillators start at the initial phase 0 and $N(1 - \eta)$ oscillators start at the initial phase π . Then $\eta = (r, \rho + 1)/2$.

D. Impact of two- and three-simplex interaction strengths

We next elucidate the impact of changes in higher-order interaction strength on the nature of dynamical evaluations, transitions points, and different basins of attraction. Figure 3 illustrates the emergence and disappearance of the stable branches in $K_1^{(1)} - r$ space for different values of $K_{2+3}^{(1)} = K_{2+3}^{(2)} = K_{2+3}$. For smaller values of K_{2+3} , there exists only one usual first-order transition route to synchronization as a function of pairwise couplings [blue solid line in Fig. 3(a)]. This transition arises due to a subcritical pitch-fork bifurcation leading to the bistable state for the simplicial layer. As K_{2+3} increases, a new pair of stable-unstable states emerges [Figs. 3(b) and 3(c)], which runs in very close vicinity (almost indistinguishable) to the existing stable coherent branch. Upon increasing K_{2+3} and further for both simplicial layers

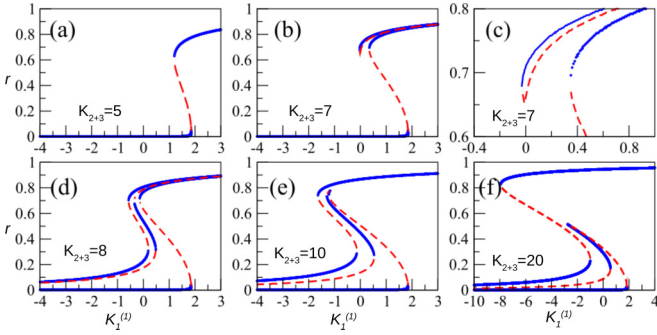


FIG. 3. Effect of higher-order interactions strength: $K_1^{(1)}$ versus r . Subfigures illustrate the emergence and disappearance of a saddle-node bifurcation leading to the emergence of the third stable state in the system for different values of K_{2+3} . (c) Zoomed part of (b) corresponding to the regime where a new branch emerges. Here $D_x = 1$ and $K_1^{(2)} = 0$.

simultaneously, this new emerged branch, which was running along the existing stable curve, joins the incoherent state gradually for large values of K_{2+3} [Fig. 3(d)]. Indeed, the previously existing stable branch gradually gets separated from the new emerging one [Figs. 3(e) and 3(f)], and then vanishes (not shown here), again restoring the same stability diagram with only one first-order transition (hysteresis) as found for the lower K_{2+3} values. Note that the figure is plotted only for particular parameter values ($D_x = 1$ and $K_1^{(2)} = 0$). However, this existence of multiple synchronization transitions is witnessed for other lower values of $K_1^{(2)}$, and also as long as a threshold value of K_{2+3} is crossed.

E. Impact of D_x : First- to second-order transition

Next, we analyze the effect of interlayer coupling strength D_x on the dynamical evolution of the individual simplicial layers. For $D_x = 0$, there exists one usual first order to synchronization and one saddle-node bifurcation in the reverse direction [9]. As simplicial layers are multilayered through D_x , multiple first-order transitions and more stable-unstable states arise. For lower values of D_x , two stable states near $r = 0$ lie in very close vicinity to each other and are indistinguishable [Fig. 4(b)] and, consequently, two forward direction first-order transitions [solid vertical lines corresponding to solid circles (blue) and open square (green)] lie very close to each other. As D_x increases gradually, two events take place; first, the hysteresis width becomes smaller [Figs. 4(a)–4(e)] and eventually vanishes, leading to a smooth second-order transition from the incoherent to the coherent state [Fig. 4(f)]. The larger D_x values intensify the impact of pairwise interlayer interactions in the entire two-layer system, driving the second-order transition to synchronization for simplicial layers. Since the pairwise couplings are known to favor synchronization among the connected nodes or, in other words, for pure s_1 complex, there endures emergence of a giant cluster with an increase in the pairwise coupling strength. This cluster attracts more and more nodes into it, leading to a second-order transition to synchronization [19]. For all nodes in the first layer connected to all nodes in the second layer, an increase in D_x readily dominates the interplay between the

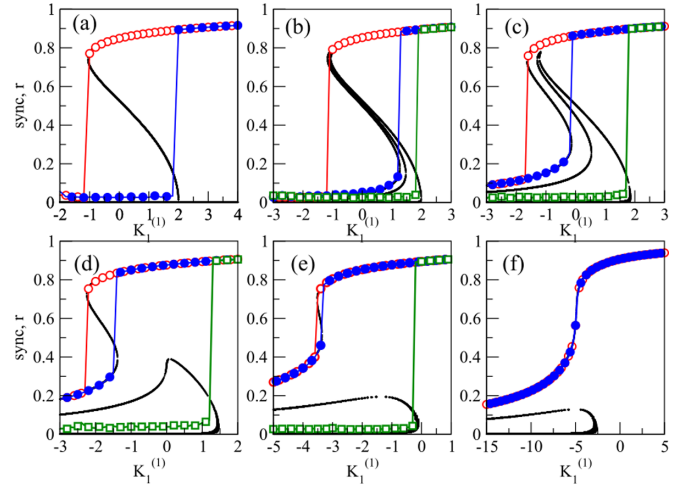


FIG. 4. Loss of hysteresis as a result of an increase in D_x . r^1 versus $K_1^{(1)}$ for $K_{2+3} = 10$. (a)–(f) Backward (red open circle) HT, forward (blue closed circle) HT and forward (green open square) WHT transitions for D_x values 0, 0.1, 0.5, 1, 2, and 3, respectively. The black solid curves represent theoretical prediction using Ott-Antonsen method depicting all stable and unstable branches.

pairwise interactions and the two- and three-simplex interactions. As a result, for large D_x values, the transition becomes purely of the second order. Second, all the transition points move toward larger negative $K_1^{(1)}$ values as D_x increases, i.e., synchronization endures for a more extensive range of $K_1^{(1)}$.

F. Dynamical evolution of the second layer

Here, we systematically analyze the importance of higher-order interactions (s_2 and s_3) in one layer in deciding a particular dynamical behavior of another layer. We demonstrate that the second layer plays a governing role in deciding the nature of the synchronization transition in the first layer. For the second layer consisting of s_2 and s_3 only, the setup leads to one more stable state in the first layer, the origin of which lies in the dynamical behavior of the second simplicial layer. Starting from $K_1^{(1)}$ values for which both the simplicial layers are in the synchronized state, as $K_1^{(1)}$ decreases, while the first layer experiences a transition to an incoherent state, the second layer, despite being extensively connected to the first layer through the pairwise interlayer connections, does not get desynchronized [Fig. 5(a)]. Next, starting with the initial condition for the phases randomly distributed between 0 and π , as $K_1^{(1)}$ increases, blue thick and black thin lines overlap with each other and together they exhibit a jump to a coherent state at $K_1^{(1)}$ 1.5 (black lines corresponding to the first layer, explained in the previous section). Next, Fig. 5(b) extends the $K_1^{(1)}$ axis, incorporating more negative values to demonstrate the robustness of the coherent behavior of the second layer against a change in $K_1^{(1)}$ values. Also, the dynamical behavior of the second simplicial layer is robust against the changes in D_x . For D_x being as high as 10, the simplicial layer does not experience any de-synchronization transition, even for very high negative $K_1^{(1)}$ values [Fig. 5(c)]. Only for very small K_{2+3} values the pure simplicial layer gets desyn-

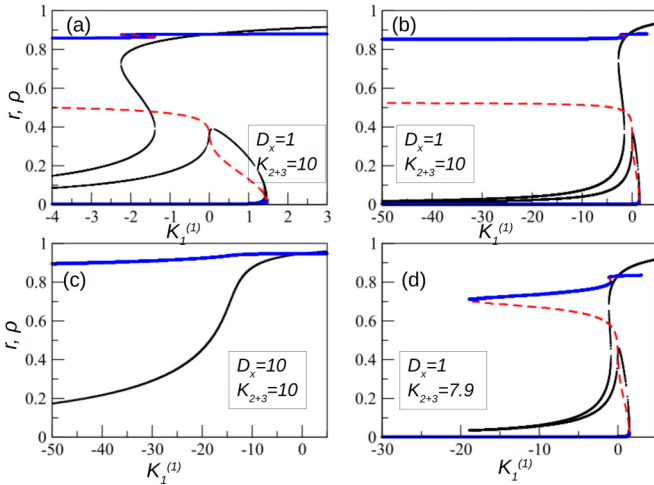


FIG. 5. Synchronization profile for the second layer (red dashed line for stable and thick blue solid line for unstable manifold) as compared to the first layer (black thin line) for both stable and unstable manifolds for different values of D_x and $K_{2+3}^{(2)}$. (a) and (b) depict robustness of ρ against a change in $K_1^{(1)}$. (b) is an extended scale of (a). (c) depicts that only one stable state exists for higher values of interlayer couplings. (d) illustrates that for a lower $K_{2+3}^{(2)}$ value, pure simplicial layer desynchronizes earlier as compared to higher $K_{2+3}^{(2)}$ [(a)–(c)].

chronized soon after the pairwise interactions in the first layer cross the origin, and that, too, this desynchronization happens much after the first layer has desynchronized [Fig. 5(d)]. Therefore, it can be concluded that dynamical behaviors of a layer consisting of pure higher-order interactions are robust against changes in the multilayering parameters.

G. Role of pure simplicial layer in the birth of multiple transitions

The absence of pairwise interactions, referred to as a pure simplicial layer, causes multiple transition routes for the order parameter of the first layer. Starting from the coherent state [green open square, Fig. 2(a)], upon adiabatically decreasing $K_1^{(1)}$, as the first layer undergoes a first-order transition to the weakly coherent state [blue open circle, Fig. 2(a)], the second layer also experiences a slight jump to a state that still is a coherent state [Fig. 5(a)]. Thereafter, the evolution of Eq. (1) with a set of the initial conditions for which the first layer lies in the weakly coherent regime and the second layer in the coherent state, with an adiabatic increase in $K_1^{(1)}$, shows hysteresis and bistability [red closed circles of Fig. 2(a)] as a consequence of the subcritical pitchfork bifurcation at λ_{c2}^f . At this critical point, the first layer jumps to the coherent state, and the second layer also keeps lying in the coherent state; ergo, both layers evolve synchronously.

III. CONCLUSION

In summary, we have reported, analytically and numerically, the emergence of stable manifolds as a consequence of connecting a simplicial layer to another simplicial layer.

Analytically, by employing the Ott-Antonsen approach, we reduced the dimensionality of the two-layer system to a set of two coupled differential equations of the order parameters of the individual layer. Such a reduction facilitates a straightforward way to comprehend the entire phase space fully and access all the bifurcation points and phase transitions, notably the existence of a third stable state. We found that an interplay of the interlayer strength and higher-order interactions brings forward several emerging dynamical behaviors, such as multiple routes to first-order transitions to synchronization accompanied by corresponding basins of attraction. With rigorous analytical calculations, we demonstrated a rich phase-space structure consisting of several stable and unstable manifolds arising from a subcritical pitch-fork and three saddle-node bifurcations. Notably, after a critical higher-order interaction strength value, connecting a simplicial layer with another simplicial layer via D_x brings upon one more stable route to the first-order transition to synchronization, in addition to the previously existing route for the isolated simplicial layer. Further, a simplicial complex without pairwise couplings does not depict a forward transition to synchronization if the initial conditions for phases are randomly drawn. Instead, it depicts a first-order transition to desynchronization in the backward direction [7]. This article has revealed that connecting such a simplicial layer to another simplicial layer brings robustness to the synchronization in the backward direction. In the absence of pairwise interactions ($K_1^{(2)} = 0$), it does not get desynchronized for the same values of the parameters for which another simplicial layer, having pairwise interactions, exhibits desynchronization.

The current article has only considered globally coupled structures for both simplicial layers, whereas real-world systems have complex underlying network architectures. A more realistic model should include such a feature among many other features inspired by real-world systems, which could be one of the future scopes of the present study. One could also relax one to all multilayer connection setups and consider a more general scheme represented by a multiplex matrix [20,21]. Further, one can include various adaptive schemes [22–24] for the simplicial interactions, for example, those inspired by the Hebbian learning in brain [10].

These findings might find applications in a range of systems having inherent multilayer architectures. It has been sufficiently emphasized that ignoring the impact of activities of nodes in one layer having one type of interaction may have wrong or inaccurate predictions of the dynamical evolution of the nodes interacting with another type of interaction. So far, all the investigations and analytical calculations on multilayer systems have considered pairwise interactions in their layers. This article, using coupled Kuramoto oscillators on simplicial multilayer systems with each layer representing globally coupled architecture as a prototype model, develops a rigorous analytical framework supported by numerical simulations. We have provided evidence of emerging dynamical behaviors, notably multiple first-order abrupt transitions to synchronization. A range of real-world complex systems, such as brain, social [25,26], financial, and technological systems, have inherent multilayer architectures [27], and their constituents units (nodes) interact with higher-order interactions forming

simplex complexes [28]. The results presented in this article, particularly the revelation of the occurrence of multiple transitions in simplicial complexes on multilayer networks, could be pivotal in predicting and comprehending the dynamics of such systems.

ACKNOWLEDGMENT

S.J. gratefully acknowledges SERB Grant No. SPF/2021/000136. We thank Saptarshi Ghosh, Ajaydeep Kachhvah, and complex systems lab members for useful suggestions.

-
- [1] L. V. Gambuzza, F. Di Patti, L. Gallo, S. Lepri, M. Romance, R. Criado, M. Frasca, V. Latora, and S. Boccaletti, *Nat. Commun.* **12**, 1255 (2021).
 - [2] A. P. Millán, J. J. Torres, and G. Bianconi, *Phys. Rev. Lett.* **124**, 218301 (2020).
 - [3] S. Majhi, M. Perc, and D. Ghosh, *J. R. Soc. Interface* **19**, 20220043 (2022).
 - [4] F. Parastesh, M. Mehrabbeik, K. Rajagopal, S. Jafari, and M. Perc, *Chaos* **32**, 013125 (2022).
 - [5] M. Manoranjani, R. Gopal, D. V. Senthilkumar, V. K. Chandrasekar, and M. Lakshmanan, *Phys. Rev. E* **105**, 034307 (2022).
 - [6] F. Battiston, E. Amico, A. Barrat, G. Bianconi, G. Ferraz de Arruda, B. Franceschiello, I. Iacopini, S. Kéfi, V. Latora, Y. Moreno, and M. M. Murray, *Nat. Phys.* **17**, 1093 (2021).
 - [7] P. S. Skardal and A. Arenas, *Phys. Rev. Lett.* **122**, 248301 (2019).
 - [8] C. Xu, X. Wang, and P. S. Skardal, *Phys. Rev. Res.* **2**, 023281 (2020).
 - [9] P. S. Skardal and A. Arenas, *Commun. Phys.* **3**, 218 (2020).
 - [10] A. D. Kachhvah and S. Jalan, *New J. Phys.* **24**, 052002 (2022).
 - [11] X. Zhang, S. Boccaletti, S. Guan, and Z. Liu, *Phys. Rev. Lett.* **114**, 038701 (2015).
 - [12] P. Khanra, P. Kundu, C. Hens, and P. Pal, *Phys. Rev. E* **98**, 052315 (2018).
 - [13] S. Jalan, A. Kumar, and I. Leyva, *Chaos* **29**, 041102 (2019).
 - [14] N. Frolov, S. Rakshit, V. Maksimenko, D. Kirsanov, D. Ghosh, and A. Hramov, *Chaos, Solitons Fractals* **147**, 110955 (2021).
 - [15] Md S. Anwar and D. Ghosh, *Chaos* **32**, 033125 (2022).
 - [16] S. Kundu and D. Ghosh, *Phys. Rev. E* **105**, L042202 (2022).
 - [17] Y. Kuramoto, Intl. Symp. Math. Prob. Theor. Phys., Lect. Notes Phys. **30**, 420 (1975).
 - [18] E. Ott and T. M. Antonsen, *Chaos* **18**, 037113 (2008).
 - [19] S. H. Strogatz, *Physica D* **143**, 1 (2000).
 - [20] A. Sole-Ribalta, M. DeDomenico, N. E. Kouvaris, A. Diaz-Guilera, S. Gomez, and A. Arenas, *Phys. Rev. E* **88**, 032807 (2013).
 - [21] A. D. Kachhvah and S. Jalan, *Phys. Rev. E* **104**, L042301 (2021).
 - [22] T. Aoki and T. Aoyagi, *Phys. Rev. Lett.* **102**, 034101 (2009).
 - [23] R. Berner, J. Sawicki, and E. Schöll, *Phys. Rev. Lett.* **124**, 088301 (2020).
 - [24] R. Berner, S. Vock, E. Schöll, and S. Yanchuk, *Phys. Rev. Lett.* **126**, 028301 (2021).
 - [25] G. Cencetti, F. Battiston, B. Lepri, and M. Karsai, *Sci. Rep.* **11**, 7028 (2021).
 - [26] F. Musciotto, F. Battiston, and R. N. Mantegna, *Commun. Phys.* **4**, 218 (2021).
 - [27] A. Aleta and Y. Moreno, *Annu. Rev. Condens. Matter Phys.* **10**, 45 (2019).
 - [28] F. Battistona, G. Cencetti, I. Iacopini, V. Latora, M. Lucas, A. Patania, J. G. Young, and G. Petri, *Phys. Rep.* **874**, 1 (2020).